Structure-activity relationship study of itraconazole, a broad-range inhibitor of picornavirus replication that targets oxysterol-binding protein (OSBP)

*Lisa Bauer[1], Salvatore Ferla[2], Sarah A. Head[3,4], Shridhar Bhat[3], Kalyan K. Pasunooti[3,5], Wei Q. Shi[3,6], Lucian Albulescu[1], Jun O. Liu[3], Andrea Brancale[2], Frank J.M. van Kuppeveld[1], Jeroen R.P.M. Strating[1]**

[1] Virology Division, Department of Infectious Diseases and Immunology, Faculty of Veterinary Medicine, Utrecht University, 3584CL Utrecht, the Netherlands

[2] Medicinal Chemistry, School of Pharmacy & Pharmaceutical Sciences, Cardiff University, King Edward VII Avenue, Cardiff CF10 3NB, UK

[3] Department of Pharmacology, Johns Hopkins School of Medicine, Baltimore, MD 21205, USA

[4] *Present address:* EMBL/CRG Systems Biology Research Unit, Centre for Genomic Regulation (CRG), Barcelona Institute of Science and Technology, Carrer del Dr. Aiguader 88, 08003 Barcelona, Spain.

[5] *Present address:* Division of Structural Biology & Biochemistry, School of Biological Sciences, Nanyang Technological University, Singapore

[6] *Present address:* Department of Chemistry and Biochemistry, University of Arkansas, Fayetteville, AR 72701, USA

* *Address for correspondence:* Jeroen R.P.M. Strating, tel +31-(0)30-2532582, j.strating@uu.nl

Abstract

Itraconazole (ITZ) is a well-known, FDA-approved antifungal drug that is also in clinical trials for its anticancer activity. ITZ exerts its anticancer activity through several disparate targets and pathways. ITZ inhibits angiogenesis by hampering the functioning of the vascular endothelial growth receptor 2 (VEGFR2) and by indirectly inhibiting mTOR signaling. Furthermore, ITZ directly inhibits the growth of several types of tumor cells by antagonizing Hedgehog signaling. Recently, we reported that ITZ also has broad-spectrum antiviral activity against enteroviruses, cardioviruses and hepatitis C virus, independent of established ITZ-activities but instead via a novel target, oxysterol-binding protein (OSBP), a cellular lipid shuttling protein. In this study, we analyzed which structural features of ITZ are important for the OSBP-mediated antiviral activity. The backbone structure, consisting of five rings, and the *sec*-butyl chain are important for antiviral activity, whereas the triazole moiety, which is critical for antifungal activity, is not. The features required for OSBP-mediated antiviral activity of ITZ overlap mostly with published features required for inhibition of VEGFR2 trafficking, but not Hh signaling. Furthermore, we use *in silico* studies to explore how ITZ could bind to OSBP. Our data show that several pharmacological activities of ITZ can be uncoupled, which is a critical step in the development of ITZ-based antiviral compounds with greater specificity and reduced off-target effects.

Keywords: Itraconazole; Encephalomyocarditis virus; Cardiovirus; Enterovirus; Molecular modeling

Introduction

Enteroviruses form a large group of viruses within the *Picornaviridae* family of positive-sense single stranded RNA (+RNA) viruses. The enteroviruses include many important human pathogens, including poliovirus (causative agent of poliomyelitis), coxsackieviruses and echoviruses (causative agents of encephalitis, meningitis, and hand, foot, and mouth disease) and rhinoviruses (causative agents of common cold, but also have a role in exacerbations of asthma and chronic obstructive pulmonary disease) (Tapparel et al., 2013). Vaccines are available against poliovirus, and an enterovirus-A71 vaccine has recently been approved in China. However, vaccination is not a feasible general strategy to prevent infections with the large amount (>250) of enterovirus (sero)types. No antiviral therapies are approved at the moment, restricting treatment of infections to supportive care. Therefore, antiviral drugs that target a broad spectrum of enteroviruses are urgently needed. Such drugs could either directly target viral proteins or act through essential host factors. Repurposing of approved drugs or compounds that have passed clinical trials, for which detailed information on safety and pharmacology is available, is an emerging alternative to the time consuming and costly *de novo* development of antiviral drugs. Recently, ITZ was identified in several drug-repurposing screens as a novel broad-spectrum anti-enteroviral agent that affects genome replication (Gao et al., 2015; Shim et al., 2016a; Strating et al., 2015). Besides enteroviruses, ITZ also inhibits picornaviruses of the *Cardiovirus* genus and hepatitis C virus, a +RNA virus belonging to the *Flaviviridae* family.

ITZ (Sporanox®) is an FDA-approved drug that is clinically used for the treatment of fungal infections. ITZ acts by inhibiting the activity of the fungal enzyme CYP51 (lanosterol 14α-demethylase), which catalyzes an essential step in the biosynthesis of cell membrane sterols, thus impairing fungal cell membrane integrity (Lestner and Hope, 2013). ITZ also inhibits the human

CYP51 isoform, although ~10-fold less potently than fungal CYP51, and the related drug metabolizing enzyme CYP3A4 (Lamb et al., 1999; Trosken et al., 2006). In drug-repurposing screens, ITZ was found to exert antitumor activity via a number of targets. ITZ directly inhibits cancer cells that depend on the Hedgehog (Hh) pathway by antagonizing Hh signaling (Kim et al., 2010). Besides, ITZ possesses potent antiangiogenic activity by indirectly inhibiting mTOR and vascular endothelial growth factor receptor 2 (VEGFR2) functioning. ITZ inhibits mTOR by targeting the mitochondrial voltage-dependent anion channel 1 (VDAC1) and the lysosomal cholesterol-binding protein Niemann-Pick disease type C1 (NPC1) (Head et al., 2015; Head et al., 2017; Trinh et al., 2017; Xu et al., 2010). ITZ interferes with the signaling activity of VEGFR2 by altering its trafficking and glycosylation (Aftab et al., 2011; Nacev et al., 2011), but the molecular target mediating this activity remains to be identified. So far, ITZ has displayed efficacy in several phase II clinical trials with patients with a number of different cancer types (Antonarakis et al., 2013; Kim et al., 2014; Rudin et al., 2013).

We previously reported that ITZ has antiviral activity (Strating et al., 2015). Since compounds that pharmacologically inhibit the other targets of ITZ do not interfere with virus replication, we concluded that the established activities of ITZ are likely unrelated to the antiviral activity. Instead, we identified oxysterol-binding protein (OSBP) as a novel target of ITZ through which the antiviral activity is exerted (Strating et al., 2015). We showed that ITZ directly binds OSBP and that other OSBP inhibitors (e.g. OSW-1) also have antiviral activity (Albulescu et al., 2015; Strating et al., 2015). Depletion of OSBP sensitized virus replication to ITZ whereas OSBP overexpression counteracted virus inhibition by ITZ, thus further strengthening our conclusion that ITZ exerts its antiviral activity via OSBP (Strating et al., 2015).

OSBP shuttles lipids at membrane contact sites (MCSs), i.e. sites where two organelles come in very close proximity, between the endoplasmic reticulum (ER) and the *trans*-Golgi apparatus (Mesmin et al., 2013). OSBP bridges the ER-Golgi MCS by simultaneously binding these two organelles. OSBP connects to the ER via an interaction of its FFAT-motif with the ER integral membrane proteins VAP-A or VAP-B. At the other side of the MCS, the PH-domain of OSBP binds the small GTPase Arf1 and phosphatidylinositol 4-phosphate [PI(4)P] lipids to connect OSBP to the *trans*-Golgi. The C-terminal OSBP-related domain (ORD) of OSBP can accommodate the lipids cholesterol and PI(4)P in its lipophilic pocket. The ORD mediates shuttling of cholesterol from the ER to the Golgi, which occurs against the concentration gradient. A concurrent shuttling of PI(4)P from the *trans*-Golgi to the ER, where PI(4)P is hydrolyzed by the phosphatase Sac1, provides the driving force for cholesterol transport. Because PI(4)P also acts as a membrane anchor for OSBP at the *trans*-Golgi, PI(4)P shuttling allows a negative feedback of OSBP localization and, as a result, activity (Mesmin et al., 2013). ITZ inhibits the cholesterol and PI(4)P shuttling activities of OSBP both *in vitro* and in cells. As a result of the inhibition of PI(4)P shuttling, ITZ prevents PI(4)P removal from the Golgi, leading to an accumulation of both PI(4)P and OSBP at ER-Golgi MCSs (Strating et al., 2015).

Like all +RNA viruses, picornaviruses rewire the cellular membrane system to generate membranous replication platforms, so-called replication organelles (ROs) (for recent reviews, see Strating and van Kuppeveld, 2017; van der Schaar et al., 2016). Each group of viruses recruits a specific set of host proteins to the ROs through viral non-structural proteins. For example, all enteroviruses recruit the Golgi-derived enzyme phosphatidylinositol 4-kinase type III β (PI4KB), which converts PI lipids into PI(4)P, leading to an enrichment of PI(4)P at ROs (Hsu et al., 2010; van der Schaar et al., 2013). The cardiovirus encephalomyocarditis virus (EMCV) instead relies

on a different isoform, namely phosphatidylinositol 4-kinase type III α (PI4KA), to generate PI(4)P-rich ROs (Dorobantu et al., 2015). The PI(4)P lipids allowing the recruitment of OSBP and drive the shuttling of cholesterol to ROs (Arita et al., 2013; Dorobantu et al., 2015; Roulin et al., 2014; Strating et al., 2015). By inhibiting the lipid shuttling activity of OSBP, ITZ hampers cholesterol transport to ROs and hence interferes with RO biogenesis and viral genome replication (Strating et al., 2015).

Here, we report a structure-activity relationship study of ITZ in which we aim to establish which structural features of ITZ are important for the inhibition of the lipid shuttling activity of OSBP and virus replication, which depends on OSBP. To study the antiviral effect of ITZ analogs, we used the cardiovirus EMCV as a model virus that is highly sensitive to ITZ (Strating et al., 2015). As a read-out for inhibition of OSBP lipid shuttling activity, we used the accumulation of OSBP at the Golgi, which is induced by the inhibition of OSBP-mediated PI(4)P shuttling from the Golgi (Strating et al., 2015). Furthermore, we performed molecular modeling studies to investigate how ITZ may bind to OSBP. We observed that the activity of the analogs towards OSBP and virus replication correlate well. Interestingly, there is overlap of antiviral activity of most analogs, except for two stereoisomers, with previously reported activity towards VEGFR2, but not Hh. Finally, our molecular modeling studies indicate that ITZ occupies the hydrophobic tunnel in the ORD which normally accommodates cholesterol and PI(4)P, thus offering a potential explanation of its mode of inhibition. Together, this study provides insight into the structural features of ITZ that are necessary for its OSBP-mediated antiviral activity, paving the way for further development of ITZ-based compounds as antiviral agents with greater specificity towards OSBP and fewer side activities (i.e. not targeting other ITZ targets such as CYP51 and Hh).

Results

Antiviral activity of ITZ and inhibition of OSBP

ITZ (Figure 1) consists of a core of five linearly linked rings (dioxolanyl-methoxyphenyl-piperazinyl-phenyl-triazolone) with substituents on either side of the core. The dioxolane ring carries a dichlorophenyl ring and a triazole moiety, the latter of which is essential for the CYP51-mediated antifungal activity. The triazolone ring on the other end of the core bears a *sec*-butyl chain that is important for the activity of ITZ towards VEGFR2 and Hh (Shi et al., 2011). ITZ has three stereogenic centers (2, 4 and 2') and thus a total of eight possible stereoisomers. To investigate the importance of different parts of ITZ for the antiviral activity, we used a small library of ITZ stereoisomers and analogs that either lacked major parts of the molecule or that had alterations in the triazole or sec-butyl moieties (Chong et al., 2007; Head et al., 2015; Shi et al., 2011; Shi et al., 2010). The antiviral activity of ITZ analogs was investigated using encephalomyocarditis virus (EMCV), a member of the *Cardiovirus* genus that, like enteroviruses, requires OSBP and is highly sensitive to ITZ (Dorobantu et al., 2015; Strating et al., 2015). HeLa cells were infected with a recombinant virus encoding a *Renilla* luciferase reporter gene (RLuc-EMCV) (Albulescu et al., 2015), treated with serial dilutions of ITZ analogs, and luciferase activity was determined as a quantitative and sensitive readout for virus replication (Figure 2A). In parallel, an MTS assay was performed to test for cytotoxicity of the compounds (Figure 2B). Technical replicates were performed as biological triplicates and EC_{50} values were calculated (Supplementary Table 1, Figure 2C). As a readout for inhibition of the lipid shuttling activity of OSBP, cells transiently expressing EGFP-tagged OSBP were treated with 10 μM of compound, fixed and imaged by fluorescence microscopy to assess the accumulation of OSBP at the Golgi (Figure 2D).

Overall, we considered compounds active when EC_{50} values were in a similar order of magnitude (i.e. less than ten-fold different from ITZ), whereas we considered them inactive when there was minimal or no inhibition at the highest concentration tested (indicated as EC_{50} values >10μM) (Tables 1-4, Supplementary Table 1, Figure 2C). In line with our previous conclusion that the antiviral activity of ITZ is mediated through OSBP (Strating et al., 2015), we observed a strong correlation between activity in the antiviral assay and the OSBP redistribution assay.

Clinically administered ITZ to treat fungal infections consists of an equimolar mixture of the four *cis*-stereoisomers (2S4R2'S; 2S4R2'R; 2R4S2'S; 2R4S2'S). All eight stereoisomers (compounds **1a-h**) clearly inhibited virus replication without notable acute cytotoxicity and induced a perinuclear OSBP accumulation indicative of an inhibition of the lipid shuttling activity of OSBP. The individual clinically administered stereoisomers (**1a-d**) had a similar potency as the clinically used ITZ mixture and were slightly more potent (up to ~8.5 fold) than the other stereoisomers (**1e-h**) (Table 1, Figure 2C). The stereoisomers in clinically used ITZ (**1a-d**) were also previously reported to be more active towards VEGFR2 glycosylation (Table 1) (Shi et al., 2011). Despite the small differences in potency, it is obvious that all eight stereoisomers are active towards OSBP and possess antiviral activity.

The triazole ring is a key feature for the antifungal effect of ITZ (Odds et al., 2003). To test the importance of the triazole ring for antiviral activity, we assayed an analog lacking the triazole ring (compound **2**), one bearing imidazole instead of triazole (compound **3**), and an analog with tetrazole (compound **4**) in place of triazole (Table 2). All compounds retained antiviral activity and induced accumulation of OSBP at the Golgi compartment, without displaying toxicity. These data indicate that the triazole moiety is not important for the antiviral activity of ITZ and that it

can be removed to reduce side effects caused by inhibition of the human CYP51 or CYP3A4 enzymes.

Next, we analyzed a group of analogs with variations in the *sec*-butyl side chain (Table 3), none of which displayed toxicity in the MTS assay. Compound **5**, which altogether lacks the *sec*-butyl chain, did not inhibit virus replication or redistribute OSBP to the Golgi. Likewise, compound **6**, which has the *sec*-butyl chain substituted with a linear side chain, was inactive towards virus replication and OSBP redistribution. In contrast, replacing the *sec*-butyl chain with a branched (compound **7**) or a cyclohexane (compound **8**) side chain did not affect the activity towards virus replication and OSBP accumulation. Together, these data indicate that a bulky, branched side chain is important for the OSBP-mediated antiviral activity of ITZ.

Finally, we tested a set of analogs that lack major parts of the dioxolane or triazolone regions (Table 4). Analogs lacking the triazolone region with its *sec*-butyl side chain (terconazole, compound **9**, compound **10**) did not redistribute OSBP or inhibit virus replication. It should be noted that we have previously shown that ketoconazole lacks antiviral activity and does not affect OSBP (Strating et al., 2015). Ketoconazole is also a clinically used antifungal drug that is virtually identical to compound **10** except that it has an imidazole ring instead of a triazole ring. However, since these analogs also lack the essential *sec*-butyl chain, we cannot discern whether this causes the lack of activity or whether the phenyl and triazolone rings in the core structure are also important. Compound **11**, which encompasses the linker and the triazolone region including the *sec*-butyl chain but lacks the dioxolane region, was also not able to redistribute OSBP and showed no antiviral effect. We previously reported that posaconazole, which is structurally highly similar to ITZ (it comprises a difluorobenzyl ring instead of a dichlorobenzyl ring, the dioxolane ring is substituted to an oxolane, and an elongated branched side chain), is also capable

of inhibiting virus replication (Strating et al., 2015). Although we cannot exclude a role for the dichlorobenzyl or the dioxolane ring moiety, our data indicate that the extensive core structure of ITZ consisting of the four linked rings is key to inhibition of OSBP and thereby the antiviral activity of ITZ.

Molecular modeling studies

We previously showed that ITZ binds OSBP directly and inhibits its lipid shuttling function, most likely by targeting the ORD (Strating et al., 2015). In order to investigate the presumed binding of ITZ to the ORD of OSBP, a series of molecular modeling studies were conducted. Currently, no structural data are available for the ORD of human OSBP or OSBP-related proteins (ORPs). Therefore, we decided to build a homology model for the OSBP ORD based on the crystal structure of the yeast ORP Osh4/Kes1p (32% identity), which essentially consists of an ORD only (Im et al., 2005). We also considered the structure of the yeast ORP Osh3, but this protein only binds PI(4)P and the binding site is too narrow to accommodate sterols. Like OSBP, Osh4 mediates an exchange of sterols for PI(4)P (de Saint-Jean et al., 2011). The structure of Osh4 has been resolved in complex with different sterols, with PI(4)P and in the apo form (de Saint-Jean et al., 2011; Im et al., 2005). The Osh4 ORD contains a hydrophobic tunnel that can accommodate sterols or one of the two fatty acyl chains of PI(4)P. Sterol binding in this tunnel induces a conformational change that shifts an amino terminal helical lid in front of the tunnel entrance (Supplementary Figure 1A). The “closed” conformation is stabilized by interactions between the lid and the sterol (Im et al., 2005). We assumed that ITZ binds in the hydrophobic tunnel of OSBP, similar to how sterols bind to ORPs. In support of our assumption that ITZ can bind in a sterol-binding pocket, ITZ has also been shown to bind NPC1 in the sterol-binding

pocket (Head et al., 2017). Based on the Osh4p structures, we reasoned that ITZ should bind to the apo form of OSBP, since ITZ would have a steric clash with the lid in the closed, sterol-binding conformation. Hence, the apo form of Osh4 was selected as a template to build a homology model of OSBP as detailed in the methods section (Supplementary Figure 1C).

We then performed molecular docking studies of ITZ into the sterol-binding pocket of OSBP. According to our models, the *sec*-butyl chain of ITZ most likely inserts deep into the hydrophobic part of the sterol-binding tunnel leaving the dioxolane ring with the triazole and dichlorobenzyl moieties outside the pocket in a more solvent exposed area. Two possible orientations were found for this part of ITZ, in one of which this part of ITZ binds proximal to the strictly conserved OSBP "fingerprint motif" EQVSHHPP, to which the head group of PI(4)P normally binds (Tong et al., 2013) (Figure 3A). Importantly, as the hydrophobic pocket is too narrow to accommodate both ITZ and lipids (sterols or one of the legs of PI(4)P), it is very likely that ITZ competitively inhibits the lipid shuttling activity of OSBP.

Importantly, the model is in agreement with the biological data obtained with the ITZ analogs. The triazole ring, positioned outside the tunnel in a solvent-exposed area, does not make specific interaction with the ORD, which is in accordance with the experimental data that the triazole ring is not important to drive accumulation of OSBP at the Golgi. We observed that the *sec*-butyl chain is fundamental for OSBP inhibition and only substitutions by bulky, non-linear side chains are tolerated. Based on our model, we conclude that a bulkier side chain better fills the narrow binding pocket at the bottom of the hydrophobic tunnel, whereas a linear alkyl chain has more flexibility in the tunnel and hence binds less tightly (Figure 3B). Finally, analogs that lacked part of the core structure of ITZ were inactive towards OSBP. In our model, the full length of the ITZ core is needed to bridge the distance between the pocket at the bottom of the hydrophobic tunnel

in which the *sec*-butyl chain docks and the outside of the tunnel where there is sufficient space to accommodate the bulky triazole-dichlorophenyl-dioxolane moiety. Shorter compounds would only fill part of the tunnel and would have significantly fewer hydrophobic interactions to stabilize them in the tunnel.

Discussion

In this study, we explored the structural features of ITZ that are important for the OSBP-mediated antiviral activity through a structure-activity relationship study and a computational model of OSBP with ITZ. All the eight ITZ stereoisomers possess inhibitory activity towards OSBP and virus replication, which is consistent with the molecular models, which predict a fairly loose fit of ITZ in the sterol-binding pocket, providing sufficient space for any of the stereoisomers. Such a loose fit is also in accordance with the strength of the interaction that we previously measured (K_d = ~400 nM) (Strating et al., 2015), which implies a relatively weak interaction. Nevertheless, we did observe that the clinically used stereoisomers were a little more potent than the non-clinically used isomers.

We observed that the triazole moiety is not important for the OSBP-mediated antiviral activity. Since the triazole moiety is essential for the antifungal activity of ITZ (Odds et al., 2003), derivatives without the triazole moiety may have potential for antiviral therapy without CYP51- or CYP3A4-mediated adverse effects or the risk of inducing resistance against triazole-class antifungals in case a patient would have a fungal co-infection. Our data clearly show the importance of the *sec*-butyl chain for OSBP-mediated antiviral activity. However, some structural variations are tolerated, as long as the side chain is branched and relatively large. Finally, the full-length core structure of ITZ appears important for the antiviral effect of ITZ to allow sufficient interactions with the hydrophobic tunnel.

Besides a broad antiviral activity, ITZ possesses a potent anticancer activity against a number of different cancer types (Aftab et al., 2011; Antonarakis et al., 2013; Rudin et al., 2013; Tsubamoto et al., 2017). So far, only the molecular targets through which ITZ inhibits the mTOR (VDAC1,

NPC-1) signaling pathway have been identified (Head et al., 2015; Head et al., 2017; Kim et al., 2010; Liang et al., 2017; Trinh et al., 2017; Tsubamoto et al., 2017). The target through which ITZ affects the trafficking, glycosylation and functioning of VEGFR2 has remained unknown. A number of ITZ analogs that we tested here, i.e. the stereoisomers and *sec*-butyl chain analogs, have previously been investigated for their effect on VEGFR2 glycosylation (which results from an inhibition of VEGFR2 trafficking and which correlates with impaired VEGFR2 functioning) and Hh signaling (as assayed using a reporter under control of the Hh-regulated transcription factor Gli1) (Shi et al., 2011). Only the *sec*-butyl chain analogs have been tested for Hh inhibition, which did not correlate with altered VEGFR2 glycosylation (Shi et al., 2011) and also does not correlate with OSBP-mediated antiviral activity (Table 3), which fits our previous conclusion that the antiviral activity of ITZ is unrelated to Hh inhibition (Strating et al., 2015). In general, our data suggest a correlation between the OSBP-mediated antiviral activity on the one hand and activity of ITZ analogs towards VEGFR2 glycosylation on the other hand (Tables 1 and 3). The *sec*-butyl chain analogs that were active towards OSBP and virus replication were also active towards VEGFR2 glycosylation (Table 3). The clinically used stereoisomers had a somewhat higher antiviral activity and affected VEGFR2 glycosylation more severely than the non-clinically used stereoisomers (Table 1) (Shi et al., 2011; Shim et al., 2016b). Only for the stereoisomers 2S4S2'R (compound **1f**) and 2R4R2'R (compound **1h**) the OSBP-mediated antiviral activity does not correlate with the previously reported effect on VEGFR2 glycosylation. At present, it is not clear whether this is truly due to different activities of those stereoisomers towards OSBP and VEGFR2 glycosylation, or whether the apparent discrepancy is caused by experimental differences (e.g. inhibitor concentrations, treatment times, cell lines, qualitative read-outs). Since we previously concluded that VEGFR2 glycosylation defect is likely unrelated

to the antiviral activity of ITZ (Strating et al., 2015), one possible explanation of our data is that inhibition of OSBP underlies the VEGFR2 glycosylation defects induced by ITZ, although future mechanistic studies (e.g. OSBP knock-down or testing additional ITZ analogs) are needed to corroborate this potential link.

If indeed ITZ affects VEGFR2 via OSBP, the trafficking, glycosylation and functioning defects of VEGFR2 may well result from disturbances of cholesterol homeostasis caused by OSBP inhibition. Such a dependence of VEGFR2 on OSBP could be directly related to the sterol shuttling activity of OSBP but may also be an indirect effect through proteins that depend on OSBP-mediated lipid homeostasis. Namely, by modulating PI(4)P levels at the Golgi, OSBP is an important regulator of the ER-Golgi MCS (Mesmin et al., 2013) and as such of other lipid transfer proteins that operate at the ER-Golgi MCS. For example, the activity of the ceramide transfer protein CERT, which shuttles ceramide to the Golgi to allow the biosynthesis of sphingomyelin, is sensitive to OSBP inhibitors (Perry and Ridgway, 2006). Presumably, by perturbing the lipid composition of the Golgi apparatus, ITZ affects the overall functioning of the Golgi, which could explain the ITZ-induced changes in VEGFR2 trafficking, glycosylation and functioning.

Together, our work contributes to the development of ITZ-derived antiviral compounds with an increased specificity towards OSBP and fewer side effects. Although it may not be possible to fully uncouple all activities of ITZ, it appears that at least OSBP-mediated antiviral activity can be uncoupled from antifungal activity (by removing or replacing the triazole group) and Hh inhibition (by altering the *sec*-butyl chain). Our computational model may facilitate medicinal chemistry optimization of ITZ because it allows to predict whether newly designed analogs can fit the hydrophobic pocket and thus exclude inactive analogs on forehand.

Experimental Section

Chemistry

ITZ has three chiral centers (designated 2, 4, 2') (Figure 1). The synthesis of all eight ITZ stereoisomers and of *sec*-butyl chain analogs (compounds **5**-**8**) has been previously described (Shi et al., 2011). The synthesis of the triazole deleted analog (compound **2**) was previously described in (Chong et al., 2007; Head et al., 2015; Shi et al., 2011; Shi et al., 2010). Compound **9** was synthesized as described in (Shi et al., 2010), and compound **11** was previously described in (Chong et al., 2007). The experimental procedure and characterization of compounds **3, 4** and **10** are described in detail in the Supplementary methods.

Cell Culture

HeLa R19 cells were grown at 37°C, 5 % CO_2 in Dulbecco's modified Eagle's medium (DMEM, Lonza) supplemented with 10 % fetal bovine serum.

Infection Assays

RLuc-EMCV, a recombinant virus encoding a *Renilla* luciferase gene upstream of the capsid-coding region, was described before (Albulescu et al., 2015; Strating et al., 2015). Virus infections were performed by incubating subconfluent HeLa R19 cells with virus at MOI 0.1 at 37°C for 30 min. Next, the medium was removed and fresh compound-containing medium was added to the cells. After 7h the medium was discarded and cells were lyzed to determine the *Renilla* luciferase activity using the *Renilla* luciferase Assay System (Promega) according to the manufacturer's protocol. Cell viability was determined in parallel using the AQueous One

Solution Cell Proliferation Assay (Promega) according to the manufacturer's protocol. The optical density at 490 nm was determined using a microplate reader.

Fluorescence Microscopy

Subconfluent HeLa R19 cells grown on coverslips in 24-well plates were transfected with 200ng per well of the pEGFP-hOSBP plasmid (Strating et al., 2015) using Fugene 6 (Promega) according to the manufacturer's instruction. After overnight expression, the medium was discarded and fresh medium containing 10μM compound was added. After 1h the cells were fixed with 4 % PFA, permeabilized with 0.1 % Triton-X100, and the nucleus was stained with DAPI as previously described (Strating et al., 2015). Cells were embedded in FluorSave (Merck Millipore) and imaged using an Olympus BX60 fluorescence microscope.

Molecular Modeling

All molecular modeling studies were performed on a Viglen Genie Intel®Core^{TM} i7-3770 vPro CPU@ 3.40 GHz x 8 running Ubuntu 14.04. Molecular Operating Environment (MOE) 2015.10 and Maestro (Schrödinger Release 2016-1) were used as molecular modeling software.

The homology model of the OSBP ORD was prepared with the MOE2015.10 homology tool using a single template approach following a procedure previously reported (Bassetto et al., 2016). The crystal structure of the ORD of Osh4p from *Saccharomyces cerevisiae* (PDB ID: 1ZI7) in the *apo* form was used as template having a sequence similarity of 32% with the human isoform (Im et al., 2005). The amino acid sequence of human OSBP was loaded in MOE together with the 3D structure of the yeast isoform and manually aligned following the reported structure-based alignment of ORDs (Tong et al., 2013), and the final 3D model was obtained as Cartesian

average of 10 generated intermediate models (Im et al., 2005). The new model was energy minimized using the Amber99 force filed and then validated in terms of the stereochemical quality of the backbone, side chain and amino acid environment using the online UCLA-DOE LAB web server. The structure of 7-hydroxycholesterol as it was co-crystallized with the ORD of Osh4 (PDB ID: 1ZHG) was inserted in the sterol-binding site of the OSBP ORD model after the superposition of the model and the crystal structure.

The new model of the ORD of human OSBP was preprocessed using the Schrödinger Protein Preparation Wizard by assigning bond orders, adding hydrogen atoms and performing a restrained energy minimization of the added hydrogen atoms using the OPLS_2005 force field. A ligands database in sdf format was prepared using MOE2015.10 and then processed using the Maestro LigPrep tool by energy minimizing the structures (OPLS_2005 force filed), generating possible ionization states at pH 7±2, generating tautomers and low-energy ring conformers. A 20 Å docking grid was prepared using as centroid the area occupied by 7-hydroxycholestrol. Molecular docking of the prepared ligands was performed using Glide standard precision (SP) keeping the default parameters and setting 5 as number of output poses per input ligand to include in the solution. The docking solutions were visual inspected in MOE2015.10 to identify the potential interaction between ligand and protein.

Acknowledgments

This work was supported by research grants from the Netherlands Organisation for Scientific Research (NWO-VENI-722.012.066 to JRPMS, NWO-VICI-91812628 to FJMvK), the European Union (Horizon 2020 Marie Skłodowska-Curie ETN 'ANTIVIRALS', grant agreement number 642434 to AB and FJMvK), the PhRMA foundation (to SAH), the US National Cancer Institute (R01CA184103 to JOL), the Flight Attendant Medical Research Institute, Prostate Cancer Foundation (to JOL), and the Johns Hopkins Institute for Clinical and Translational Research (ICTR), which is funded in part by Grant Number UL1 TR 001079. SF and AB acknowledge support from the Life Science Research Network Wales grant no. NRNPGSep14008, an initiative funded through the Welsh Government's Ser Cymru program.

References

Aftab, B.T., Dobromilskaya, I., Liu, J.O., Rudin, C.M., 2011. Itraconazole inhibits angiogenesis and tumor growth in non-small cell lung cancer. Cancer Res. 71, 6764-6772.

Albulescu, L., Strating, J.R., Thibaut, H.J., van der Linden, L., Shair, M.D., Neyts, J., van Kuppeveld, F.J., 2015. Broad-range inhibition of enterovirus replication by OSW-1, a natural compound targeting OSBP. Antiviral Res. 117, 110-114.

Antonarakis, E.S., Heath, E.I., Smith, D.C., Rathkopf, D., Blackford, A.L., Danila, D.C., King, S., Frost, A., Ajiboye, A.S., Zhao, M., Mendonca, J., Kachhap, S.K., Rudek, M.A., Carducci, M.A., 2013. Repurposing itraconazole as a treatment for advanced prostate cancer: a noncomparative randomized phase II trial in men with metastatic castration-resistant prostate cancer. Oncologist 18, 163-173.

Arita, M., Kojima, H., Nagano, T., Okabe, T., Wakita, T., Shimizu, H., 2013. Oxysterol-binding protein family I is the target of minor enviroxime-like compounds. J. Virol. 87, 4252-4260.

Bassetto, M., Ferla, S., Pertusati, F., Kandil, S., Westwell, A.D., Brancale, A., McGuigan, C., 2016. Design and synthesis of novel bicalutamide and enzalutamide derivatives as antiproliferative agents for the treatment of prostate cancer. Eur. J. Med. Chem. 118, 230-243.

Chong, C.R., Xu, J., Lu, J., Bhat, S., Sullivan, D.J., Jr., Liu, J.O., 2007. Inhibition of angiogenesis by the antifungal drug itraconazole. ACS Chem. Biol. 2, 263-270.

de Saint-Jean, M., Delfosse, V., Douguet, D., Chicanne, G., Payrastre, B., Bourguet, W., Antonny, B., Drin, G., 2011. Osh4p exchanges sterols for phosphatidylinositol 4-phosphate between lipid bilayers. J. Cell Biol. 195, 965-978.

Dorobantu, C.M., Albulescu, L., Harak, C., Feng, Q., van Kampen, M., Strating, J.R., Gorbalenya, A.E., Lohmann, V., van der Schaar, H.M., van Kuppeveld, F.J., 2015. Modulation of the host lipid landscape to promote RNA virus replication: The picornavirus encephalomyocarditis virus converges on the pathway used by hepatitis C virus. PLoS Pathog. 11, e1005185.

Gao, Q., Yuan, S., Zhang, C., Wang, Y., Wang, Y., He, G., Zhang, S., Altmeyer, R., Zou, G., 2015. Discovery of itraconazole with broad-spectrum in vitro antienterovirus activity that targets nonstructural protein 3A. Antimicrob. Agents Chemother. 59, 2654-2665.

Head, S.A., Shi, W., Zhao, L., Gorshkov, K., Pasunooti, K., Chen, Y., Deng, Z., Li, R.J., Shim, J.S., Tan, W., Hartung, T., Zhang, J., Zhao, Y., Colombini, M., Liu, J.O., 2015. Antifungal drug itraconazole targets VDAC1 to modulate the AMPK/mTOR signaling axis in endothelial cells. Proc. Natl. Acad. Sci. U. S. A. 112, E7276-7285.

Head, S.A., Shi, W.Q., Yang, E.J., Nacev, B.A., Hong, S.Y., Pasunooti, K.K., Li, R.J., Shim, J.S., Liu, J.O., 2017. Simultaneous targeting of NPC1 and VDAC1 by itraconazole leads to synergistic inhibition of mTOR signaling and angiogenesis. ACS Chem. Biol. 12, 174-182.

Hsu, N.Y., Ilnytska, O., Belov, G., Santiana, M., Chen, Y.H., Takvorian, P.M., Pau, C., van der Schaar, H., Kaushik-Basu, N., Balla, T., Cameron, C.E., Ehrenfeld, E., van Kuppeveld, F.J., Altan-Bonnet, N., 2010. Viral reorganization of the secretory pathway generates distinct organelles for RNA replication. Cell 141, 799-811.

Im, Y.J., Raychaudhuri, S., Prinz, W.A., Hurley, J.H., 2005. Structural mechanism for sterol sensing and transport by OSBP-related proteins. Nature 437, 154-158.

Kim, D.J., Kim, J., Spaunhurst, K., Montoya, J., Khodosh, R., Chandra, K., Fu, T., Gilliam, A., Molgo, M., Beachy, P.A., Tang, J.Y., 2014. Open-label, exploratory phase II trial of oral itraconazole for the treatment of basal cell carcinoma. J. Clin. Oncol. 32, 745-751.

Kim, J., Tang, J.Y., Gong, R., Kim, J., Lee, J.J., Clemons, K.V., Chong, C.R., Chang, K.S., Fereshteh, M., Gardner, D., Reya, T., Liu, J.O., Epstein, E.H., Stevens, D.A., Beachy, P.A., 2010. Itraconazole, a commonly used antifungal that inhibits Hedgehog pathway activity and cancer growth. Cancer Cell 17, 388-399.

Lamb, D.C., Kelly, D.E., Waterman, M.R., Stromstedt, M., Rozman, D., Kelly, S.L., 1999. Characteristics of the heterologously expressed human lanosterol 14alpha-demethylase (other names: P45014DM, CYP51, P45051) and inhibition of the purified human and Candida albicans CYP51 with azole antifungal agents. Yeast 15, 755-763.

Lestner, J., Hope, W.W., 2013. Itraconazole: an update on pharmacology and clinical use for treatment of invasive and allergic fungal infections. Expert Opin. Drug Metab. Toxicol. 9, 911-926.

Liang, G., Liu, M., Wang, Q., Shen, Y., Mei, H., Li, D., Liu, W., 2017. Itraconazole exerts its anti-melanoma effect by suppressing Hedgehog, Wnt, and PI3K/mTOR signaling pathways. Oncotarget 8, 28510-28525.

Mesmin, B., Bigay, J., Moser von Filseck, J., Lacas-Gervais, S., Drin, G., Antonny, B., 2013. A four-step cycle driven by PI(4)P hydrolysis directs sterol/PI(4)P exchange by the ER-Golgi tether OSBP. Cell 155, 830-843.

Nacev, B.A., Grassi, P., Dell, A., Haslam, S.M., Liu, J.O., 2011. The antifungal drug itraconazole inhibits vascular endothelial growth factor receptor 2 (VEGFR2) glycosylation, trafficking, and signaling in endothelial cells. J. Biol. Chem. 286, 44045-44056.

Odds, F.C., Brown, A.J., Gow, N.A., 2003. Antifungal agents: mechanisms of action. Trends Microbiol. 11, 272-279.

Perry, R.J., Ridgway, N.D., 2006. Oxysterol-binding protein and vesicle-associated membrane protein-associated protein are required for sterol-dependent activation of the ceramide transport protein. Mol. Biol. Cell 17, 2604-2616.

Roulin, P.S., Lotzerich, M., Torta, F., Tanner, L.B., van Kuppeveld, F.J., Wenk, M.R., Greber, U.F., 2014. Rhinovirus uses a phosphatidylinositol 4-phosphate/cholesterol counter-current for the formation of replication compartments at the ER-Golgi interface. Cell Host Microbe 16, 677-690.

Rudin, C.M., Brahmer, J.R., Juergens, R.A., Hann, C.L., Ettinger, D.S., Sebree, R., Smith, R., Aftab, B.T., Huang, P., Liu, J.O., 2013. Phase 2 study of pemetrexed and itraconazole as second-line therapy for metastatic nonsquamous non-small-cell lung cancer. J. Thorac Oncol. 8, 619-623.

Shi, W., Nacev, B.A., Aftab, B.T., Head, S., Rudin, C.M., Liu, J.O., 2011. Itraconazole side chain analogues: structure-activity relationship studies for inhibition of endothelial cell proliferation, vascular endothelial growth factor receptor 2 (VEGFR2) glycosylation, and hedgehog signaling. J. Med. Chem. 54, 7363-7374.

Shi, W., Nacev, B.A., Bhat, S., Liu, J.O., 2010. Impact of absolute stereochemistry on the antiangiogenic and antifungal activities of itraconazole. ACS Med. Chem. Lett. 1, 155-159.

Shim, A., Song, J.H., Kwon, B.E., Lee, J.J., Ahn, J.H., Kim, Y.J., Rhee, K.J., Chang, S.Y., Cha, Y., Lee, Y.S., Kweon, M.N., Park, K.S., Kim, D.E., Cho, S., Cho, H.J., Ko, H.J., 2016a. Therapeutic and prophylactic activity of itraconazole against human rhinovirus infection in a murine model. Sci. Rep. 6, 23110.

Shim, J.S., Li, R.J., Bumpus, N.N., Head, S.A., Kumar Pasunooti, K., Yang, E.J., Lv, J., Shi, W., Liu, J.O., 2016b. Divergence of antiangiogenic activity and hepatotoxicity of different stereoisomers of itraconazole. Clin. Cancer Res. 22, 2709-2720.

Strating, J.R., van der Linden, L., Albulescu, L., Bigay, J., Arita, M., Delang, L., Leyssen, P., van der Schaar, H.M., Lanke, K.H., Thibaut, H.J., Ulferts, R., Drin, G., Schlinck, N., Wubbolts, R.W., Sever, N., Head, S.A., Liu, J.O., Beachy, P.A., De Matteis, M.A., Shair, M.D., Olkkonen, V.M., Neyts, J., van Kuppeveld, F.J., 2015. Itraconazole inhibits enterovirus replication by targeting the oxysterol-binding protein. Cell Rep. 10, 600-615.

Strating, J.R., van Kuppeveld, F.J., 2017. Viral rewiring of cellular lipid metabolism to create membranous replication compartments. Current Opin. Cell Biol. 47, 24-33.

Tapparel, C., Siegrist, F., Petty, T.J., Kaiser, L., 2013. Picornavirus and enterovirus diversity with associated human diseases. Infect. Genet. Evol. 14, 282-293.

Tong, J., Yang, H., Yang, H., Eom, S.H., Im, Y.J., 2013. Structure of Osh3 reveals a conserved mode of phosphoinositide binding in oxysterol-binding proteins. Structure 21, 1203-1213.

Trinh, M.N., Lu, F., Li, X., Das, A., Liang, Q., De Brabander, J.K., Brown, M.S., Goldstein, J.L., 2017. Triazoles inhibit cholesterol export from lysosomes by binding to NPC1. Proc. Natl. Acad. Sci. U. S. A. 114, 89-94.

Trosken, E.R., Adamska, M., Arand, M., Zarn, J.A., Patten, C., Volkel, W., Lutz, W.K., 2006. Comparison of lanosterol-14 alpha-demethylase (CYP51) of human and Candida albicans for inhibition by different antifungal azoles. Toxicology 228, 24-32.

Tsubamoto, H., Inoue, K., Sakata, K., Ueda, T., Takeyama, R., Shibahara, H., Sonoda, T., 2017. Itraconazole Inhibits AKT/mTOR Signaling and proliferation in endometrial cancer cells. Anticancer Res. 37, 515-519.

Van der Schaar, H.M., Dorobantu, C.M., Albulescu, L., Strating, J.R., van Kuppeveld, F.J., 2016. Fat(al) attraction: Picornaviruses usurp lipid transfer at membrane contact sites to create replication organelles. Trends Microbiol. 24, 535-546.

Van der Schaar, H.M., Leyssen, P., Thibaut, H.J., de Palma, A., van der Linden, L., Lanke, K.H., Lacroix, C., Verbeken, E., Conrath, K., Macleod, A.M., Mitchell, D.R., Palmer, N.J., van de Poel, H., Andrews, M., Neyts, J., van Kuppeveld, F.J., 2013. A novel, broad-spectrum inhibitor of enterovirus replication that targets host cell factor phosphatidylinositol 4-kinase IIIbeta. Antimicrob. Agents Chemother. 57, 4971-4981.

Xu, J., Dang, Y., Ren, Y.R., Liu, J.O., 2010. Cholesterol trafficking is required for mTOR activation in endothelial cells. Proc. Natl. Acad. Sci. U. S. A. 107, 4764-4769.

Figure legends

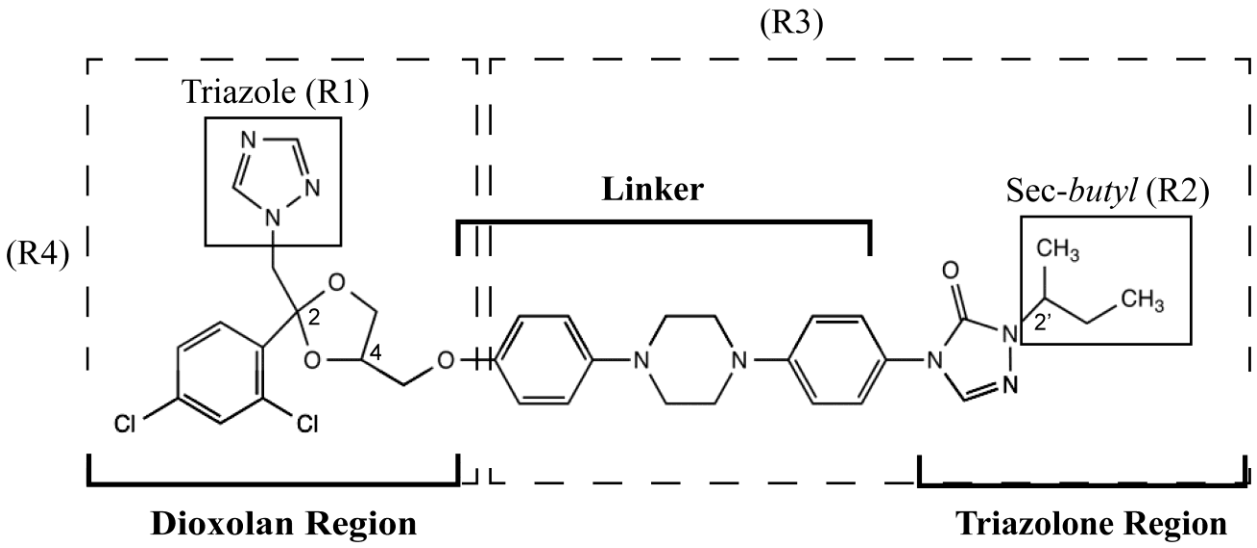

Figure 1. Structure of ITZ.

ITZ has three stereogenic centers (2, 4 and 2'), giving rise to eight different stereoisomers. The boxes indicate the side-chains that are changed in the tested analogs.

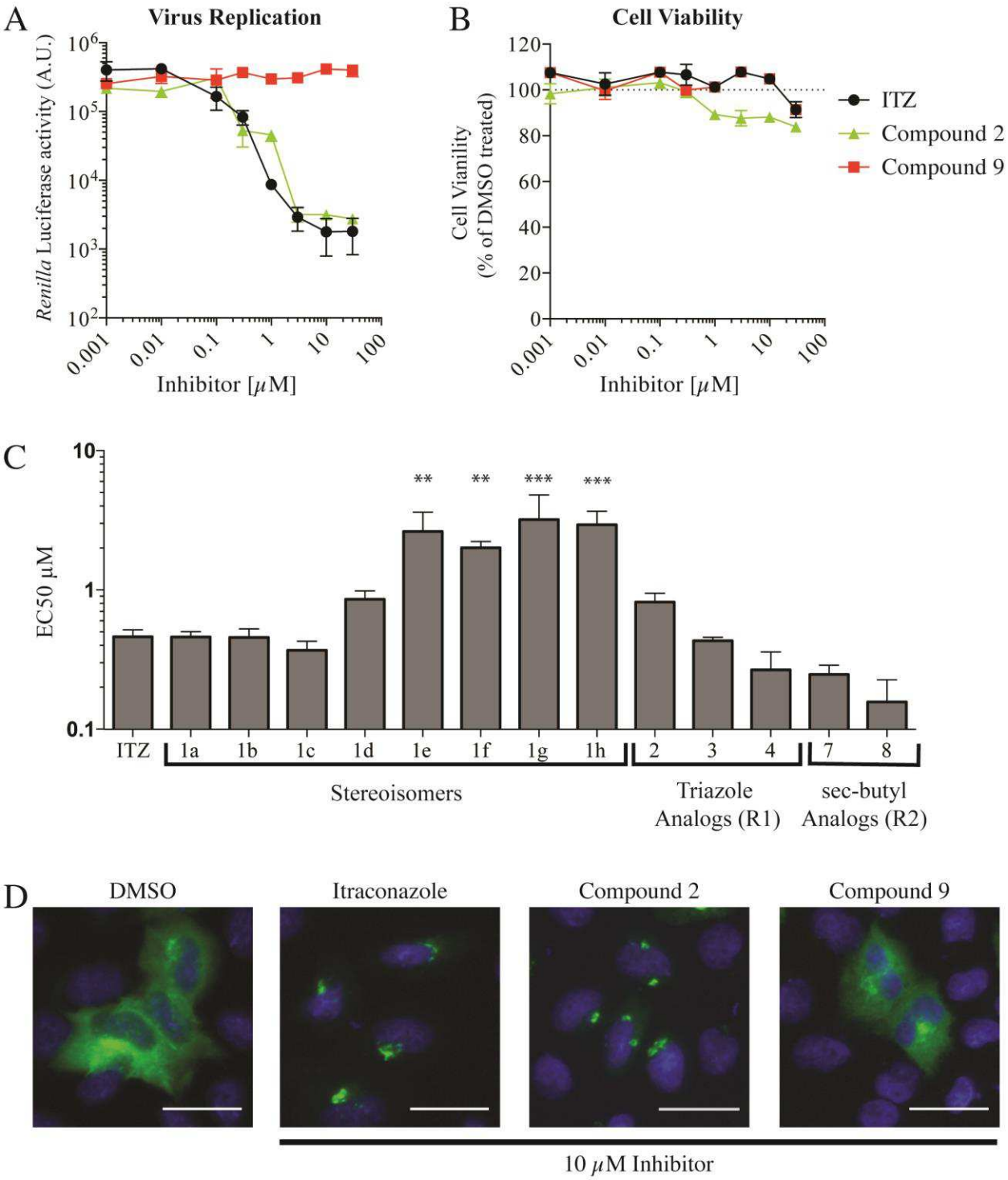
A
Virus Replication
Renilla Luciferase activity (A.U.)
Inhibitor [μM]
B
Cell Viability
Cell Vianility (% of DMSO treated)
Inhibitor [μM]
ITZ
Compound 2
Compound 9
C
EC50 μM
ITZ
1a
1b
1c
1d
1e
1f
1g
1h
2
3
4
7
8
Stereoisomers
Triazole Analogs (R1)
sec-butyl Analogs (R2)
D
DMSO
Itraconazole
Compound 2
Compound 9
10 μM Inhibitor

Figure 2. The effects of ITZ analogs on virus replication and OSBP redistribution.

(A) HeLa R19 cells were infected with a *Renilla* luciferase (RLuc)-EMCV reporter virus, treated with compounds, and luciferase activity was determined as a quantitative measure of replication. Shown are ITZ as a positive control, and one representative example each of an active (compound **2**) and an inactive (compound **9**) analog. (B) In parallel, uninfected cells were treated with compound and cell viability was determined using an MTS assay. Experiments in (A) and (B) were performed as biological triplicates and mean values ± SEM are shown. (C) Up to four independent technical replicates (each performed as biological triplicates) were performed and EC_{50} values were calculated for each replicate (Supplementary Table 1) (except compounds **1c**, **1e** and **1g**). Mean EC_{50} values and SD are plotted and analyzed by one-way ANOVA with Bonferroni's post hoc test. Asterisks indicate statistically significant differences compared to ITZ (**, $p<0.01$; ***, $p<0.001$). Bars without asterisks are statistically not significantly different from ITZ. (D) HeLa R19 cells were transfected with a plasmid encoding EGFP-OSBP and treated for 1h with 10 μM compound. Cells were fixed, counterstained with DAPI to visualize the nuclei (blue) and imaged for OSBP localization using fluorescence microscopy. Only compounds that inhibit virus replication induce OSBP accumulation (see also Tables 1-4). Representative examples of independent technical replicates are shown. Scale bars correspond to 50 μm.

Figure 3. Modeling of the OSBP ORD structure with ITZ.

(A) Homology model of the OSBP ORD in the open conformation. The *sec*-butyl chain of ITZ inserts deep in the hydrophobic tunnel, leaving the triazole-dichlorophenyl-dioxolane region outside in a more solvent exposed area. Our models calculated two possible orientations for this part (the two different models for ITZ are shown as yellow and light green carbon atoms respectively), one of which is in proximity of the strictly conserved "OSBP fingerprint motif" EQVSHHPP (lilac surface). The position of 7-hydroxycholesterol is shown in purple. (B) Zoom into the binding pocket of ITZ, only one calculated orientation of ITZ is shown.

Tables

Table 1. The activity of ITZ stereoisomers

Means and standard deviations are from at least four independent technical replicates (except 1c, 1e and 1g, which were tested twice), each performed as biological triplicates.
[a] *Stereoisomers included in clinically administered ITZ.*
[b] *Data from Shi et al., 2011.*
[c] *Inhibition of Hh signaling, determined using a reporter for the Hh-regulated transcription factor Gli1 (Shi et al., 2011).*
n.d.; not determined.

Compound	Inhibition of virus replication EC_{50} ± SD (μM)	OSBP redistribution (10 μM)	VEGFR2 glycosylation[b] (2 μM)	Hh inhibition[c]

ITZ	0,46 ± (0,14)	+	++	++
1a (2S4R2'S)[a]	0,46 ± (0,08)	+	++	n.d.
1b (2S4R2'R)[a]	0,46 ± (0,12)	+	++	n.d.
1c (2R4S2'S)[a]	0,37 ± (0,06)	+	++	n.d.
1d (2R4S2'R)[a]	0,86 ± (0,22)	+	++	n.d.
1e (2S4S2'S)	2,63 ± (0,99)	+	+	n.d.
1f (2S4S2'R)	2,01 ± (0,38)	+	-	n.d.
1g (2R4R2'S)	3,21 ± (1,61)	+	+	n.d.
1h (2R4R2'R)	2,95 ± (1,26)	+	-	n.d.

Table 2. The activity of ITZ triazole-moiety analogs

Means and standard deviations are from at least four independent technical replicates, each performed as biological triplicates.
[a] Data from (Shi et al., 2011).
[b] Inhibition of Hh signaling, determined using a reporter for the Hh-regulated transcription factor Gli1 Shi et al., 2011.
n.d.; not determined.

Compound	R1	Inhibition of virus replication EC_{50} ± SD (μM)	OSBP redistribution (10 μM)	VEGFR2 glycosylation[a] (2 μM)	Hh inhibition[b]
ITZ	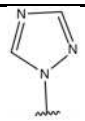	0,46 ± (0,14)	+	++	++
2		0,82 ± (0,22)	+	n.d.	n.d.
3	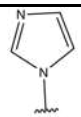	0,43 ± (0,04)	+	n.d.	n.d.
4	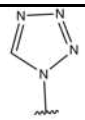	0,26 ± (0,16)	+	n.d.	n.d.

Table 3. The activity of ITZ *sec*-butyl chain analogs

Means and standard deviations are from at least four independent technical replicates, each performed as biological triplicates.
[a] Data from (Shi et al., 2011).
[b] Inhibition of Hh signaling, determined using a reporter for the Hh-regulated transcription factor Gli1 (Shi et al., 2011).

Compound	R2	Inhibition of virus replication EC_{50} ± SD (μM)	OSBP redistribution (10 μM)	VEGFR2 glycosylation (2 μM)[a]	Hh inhibition [b]
ITZ	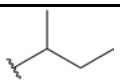	0,46 ± (0,14)	+	++	++
5		> 10	-	-	++
6		> 10	-	-	-
7	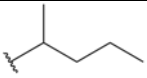	0,25 ± (0,07)	+	++	++
8	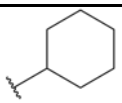	0,16 ± (0,12)	+	++	-

Table 4. The activity of ITZ analogs with changes in the core structure

Means and standard deviations are from at least three independent technical replicates, each performed as biological triplicates.
[a] *Compounds with changes in R3*
[b] *Compounds with changes in R4*
[c] *Data for ITZ from (Shi et al., 2011), data for Terconazole from (Nacev et al., 2011).*
[d] *Inhibition of Hh signaling, determined using a reporter for the Hh-regulated transcription factor Gli1 (Shi et al., 2011).*
n.d.; not determined.

Compound	R3 / R4	Inhibition of virus replication EC_{50} ± SD (μM)	OSBP redistribution (10 μM)	VEGFR2 glycosylation (2 μM)[c]	Hh inhibition[d]
ITZ		0,46 ± (0,14)	+	+	++
Terconazole [a]	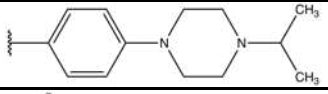	> 10	-	-	n.d.
9[a]	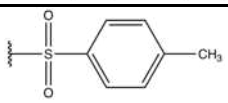	> 10	-	n.d.	n.d.
10[a]	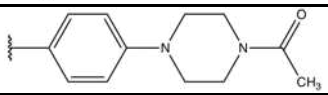	> 10	-	n.d.	n.d.
11[b]		> 10	-	n.d.	n.d.